1D MONTE-CARLO SIMULATION OF CHAREGE ACCUMULATION PROCESS INSIDE TEFLON® FILM

R. Watanabe, M. Ota, Y. Tanaka and N. Tomita

Dept. of Mechanical Systems Eng., Musashi Institute of Technology
1-28-1, Tamazutsumi, Setagaya, Tokyo, 158-8557, JAPAN
TEL: +81-3-3703-3111, FAX: +81-3-5707-1180
E-mail:rwata@sc.musashi-tech.ac.jp

ABSTRACT

The charge accumulation processes inside a Teflon film are investigated with one-dimensional Monte-Carlo simulation. Elastic and inelastic scattering processes are considered in the collisions between electrons and atoms consisting of Teflon® (CF4). Electron-phonon interaction and trapping effect are also included in the estimation of total cross section. A case of 20 keV electron irradiation is tested and charge accumulation process is successfully simulated. The electric field is also calculated based on the one-dimensional Poisson equations. The formation of strong electric field induced by the electron charge is clearly seen. The computed charge density distributions are compared with other simulation results and experimental data. The innovative measurement technique is used to obtain the charge density distribution inside a Teflon film. A PC based parallel computer is introduced to accelerate the computation so that the realistic time scale is attained.

INTRODUCTION

Dielectric breakdowns and electrostatic discharges occurring on/inside spacecraft surfaces have been considered as one of major causes of spacecraft malfunction and failures [1]. These concerns are heightened for GEO (GEosynchronous Orbit) that can suffer from severe bombardment of high-energy electrons and other charged particles. In order to avoid failures, detailed analyses of charging and discharging process inside surface materials such as Teflon® are essential. Most previous studies focused on surface charging in a low-energy plasma environment and theorized that differential surface charging may result in catastrophic discharges [2]. Recently, however, it has been pointed out that besides surface charging there is possibility that internal charging is also related to discharging of spacecraft [3]. Although there are some practical estimations of discharge criteria based on empirical equations [4], numerical simulations based on first principle are important to understand the phenomena. Clarifying the charge accumulation process inside insulating polymers will assist in the analysis of spacecraft failures and allow the prediction and prevention of dielectric breakdowns that might occur under severe electron irradiation in space.

In the present research, the charge accumulation processes inside a Teflon film are investigated by a combination of computational and experimental methods. The simulation strategy is based on the Monte Carlo methodology to address collisional processes. Each injected electron is tracked three-dimensionally based on the quantum consideration of the elastic and inelastic scattering processes between electrons and atoms consisting of Teflon (CF_4) described by Palov et al [5]. Electron-phonon interaction and trapping effect are also included in the estimation of total cross section. Simulation results of an incident electron beam with energy of 20 keV are presented. In order to verify the computations, electron irradiation experiments are conducted based on a measurement technique described by Watanabe et al [6]. Real-time measurements of the charge distributions inside Teflon are also presented.

PHYSICAL MODEL

Collision processes between electrons and Teflon are modeled following Palov et al [5]. Electron energies are in the range of 1 eV to 35 keV and the processes considered in the model are: (i) electron scattering by C or F atoms, (ii) ionization of atoms, (iii) electron-phonon interaction and (iv) trapping. Palov et al derives these formulae from quantum electro dynamics and other experimental results. The cross sections of each process are calculated in advance as a function of the electron energy.

(i) Elastic Electron Scattering

Electron scattering in Teflon is considered separately with Carbon (C) and Fluorine (F) atoms because the theory of electron-molecule collision process has not been adequately developed. The mean free path for elastic collision λ_{el}^{-1} is calculated from

$$\lambda_{el}^{-1} = \frac{4\pi n}{k^2}\sum_{l=0}^{\infty}(2l+1)\sin^2\delta_l , \tag{1}$$

where n is the number density of atoms in Teflon and k is the electron wave vector. The phase shifts δ_l were obtained by calculating the following differential equation,

$$\frac{d\delta_l}{dR} = -\frac{V(k,R)}{k}\left|\cos\delta_l\,\hat{\mathrm{j}}_l(kR) - \sin\delta_l\,\hat{\mathrm{n}}_l(kR)\right|^2 , \tag{2}$$

$$V(k,R) = V_{static}(R) + V_{exchange}(k,R) + V_{corr}(R) . \tag{3}$$

where $\hat{\mathrm{j}}_l(kR)$ and $\hat{\mathrm{n}}_l(kR)$ are spherical Bessel and Neumann functions of order l and R is the distance from the center of the atomic core. Detailed descriptions for the potentials $V_{static}(R), V_{exchange}(k,R)$ and $V_{corr}(R)$ are given in Ref. [5].

The azimuthal φ and polar θ scattering angles are calculated based on the following double cross section equation,

$$\frac{d^2\lambda_{el}^{-1}}{d(-\cos\theta)d\varphi} = \frac{n}{2\pi k^2}\left|\sum_{l=0}^{\infty}(2l+1)\sin\delta_l\exp(i\delta_l)P_l(\cos\theta)\right|^2 , \tag{4}$$

where $P_l(\cos\theta)$ is the l-th Legendre polynomial.

(ii) Ionization of Atoms and Generation of Secondary Electrons

The ionization of the inner atomic shells and a valence band are dominant as inelastic scattering processes especially in a higher energy range. We used the classical theory of binary collision for the description of the ionization of inner atomic shells and the generation of secondary electrons. The inelastic mean free path before ionization of the j-th shell λ_i and electron energy losses are calculated from differential cross sections averaged over kinetic energies of shell electrons,

$$\frac{d\lambda_i^{-1}}{dy} = \frac{\pi a_0^2 n N_j}{U_j^{2^*}y^3}\left\{(1-y/x)^{\frac{1}{1+y}}\left[y(1-1/x)+\frac{4}{3}\ln\left(2.7+\sqrt{x-y}\right)\right]\sqrt{\frac{x}{(1+x)^3}}\right\}, \tag{5}$$

where $x = E/U_j$, $y = \Delta E/U$, E is the energy of a primary electron, ΔE is its energy loss, n is atomic concentration, N_j is the quantity of electrons on the j-th shell and U_j (in atomic units) is the binding energy of the j-th shell and a_0 is the Bohr radius. The momentum loss ΔP of a primary electron is estimated by the following double differential cross section for a fixed kinetic energy of a shell electron,

$$\frac{d^2\lambda_i^{-1}}{dyd\xi} = \frac{\pi a_0^2 nN}{8\sqrt{2x}E^2}\xi^{-5/2}$$

$$\xi = 1 - y/2x - \sqrt{1-y/x}\cos\theta\,,\ \Delta P = 2E\xi \tag{6}$$

$$E_1 = E - \Delta E,\ E_s = \Delta E - U_j + \chi \tag{7}$$

where E is in atomic units. E_1 is the energy of the primary electron after collision and E_2 is the energy of the secondary electron, where χ is the electron affinity of Teflon.

Polar angles of the primary and secondary electrons are calculated from Eq. (6) and the energy and momentum conservation laws. The azimuthal angle φ of the primary electron is uniformly distributed in the $(0,2\varphi)$ interval, the secondary one φ_s is connected with φ by

$$\cos(\varphi-\varphi_s)=\frac{(p-c)(p_i\cos\phi-c)}{t\sqrt{(p^2-c^2)}}$$
$$c=(2p^2-2m\Delta E-\Delta P^2)/2p,\quad p=\sqrt{2mE},$$
$$t^2=2m\Delta E+p_j^2-(p+p_j\cos\phi-c)^2,\quad p_j=\sqrt{2mU_j}, \tag{8}$$

where ϕ is the angle between atomic and primary electron velocities before a collision and m is the electron mass.

(iii) Electron-Phonon Interaction

The electron-phonon interaction is also included in the model because it is important when electron energy is less than the energy gap. We used Frohlich's formulas [7] to estimate the mean free path of an electron before the creation of a phonon λ_{ph}^{-1}.

$$\frac{d\lambda_{ph}^{-1}}{dq}=\frac{(1+n_q)}{2a_0}\frac{E_{ph}}{E}\left(\frac{1}{\varepsilon_\infty}-\frac{1}{\varepsilon_0}\right)\frac{1}{q}$$
$$q_{\min}=\frac{\sqrt{2m}}{\hbar}\left(\sqrt{E}-\sqrt{E_{ph}}\right)$$
$$q_{\max}=\frac{\sqrt{2m}}{\hbar}\left(\sqrt{E}+\sqrt{E-E_{ph}}\right) \tag{9}$$

where E_{ph} is the energy of a fixed longitudinal optical phonon ε_0 and ε_∞ are the insulator dielectric functions in zero and high energy limits. q is the wave vector lost by an electron in the process of the creation of a longitudinal phonon, $n_q=\{\exp(E_{ph}/KT)-1\}^{-1}$, K is the Boltzmann constant and T is the temperature of the insulator.

(iv) Polaronic Effect and Electron Trapping

The polaronic effect is important because it describes electron trapping and detrapping inside insulators especially when they have lower energy. We used a semi-empirical method [8] to calculate the mean free path before trapping λ_{trap}^{-1},

$$\lambda_{trap}^{-1}=a\exp(-E/b) \tag{10}$$

where a =1 nm^{-1} and b = 1.5 eV. The parameters a and b were adjusted according to the calculated TSEY with experimental data.

PARTICLE TRACKING AND FIELD CALCULATION

Injected electron particles move through the target material with energy attenuation due to the inelastic collision described above. The motion between the collision processes encountered is simulated by the non relativistic equations of motion i.e. the Newton's equations of motion. The effect of electric field induced by the accumulated charge is included. The three-dimensional position vector of electron particle $\mathbf{r}$ and its velocity vector $\mathbf{v}$ are updated on each uniform times step τ as follows.

$$\mathbf{r}_{new}=\mathbf{r}_{old}+\mathbf{v}_{old}\tau+\left(\frac{e}{m}\right)\mathbf{E}_{old}\left(\frac{\tau^2}{2}\right) \tag{11}$$

$$\mathbf{v}_{new}=\mathbf{v}_{old}+\left(\frac{e}{m}\right)\mathbf{E}_{old}\tau \tag{12}$$

$$\tau = \frac{\lambda_{total}}{\mathbf{v}_{old}} \tag{13}$$

where, e is the elementary charge, m is the electron mass, $\mathbf{E}$ is the electric field inside the material and λ_{total} is the total mean free path between the successive collisions calculated from above mentioned mean free paths.

$$\lambda_{total}^{-1} = \lambda_{elC}^{-1} + \lambda_{elF}^{-1} + \sum_{j=1}^{3}(\lambda_{iC}^{-1} + \lambda_{iF}^{-1})j + \lambda_{ph}^{-1} + \lambda_{trap}^{-1} \tag{14}$$

Once three-dimensional electron distribution is determined, one-dimensional charge distribution $\rho(x)$ can be calculated on the mesh indicated in the simulated model Fig. 1. The electric field $E(x)$ (and also electric potential $\phi(x)$) are obtained by integrating the following Poisson's equations,

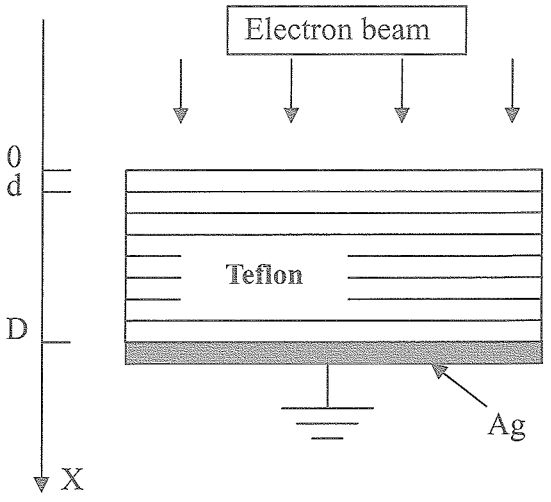

FIGURE 1. Simulated model

$$\frac{dE(x)}{dx} = \frac{1}{\varepsilon_0 \varepsilon}\rho(x) \tag{15}$$

$$\frac{d\phi(x)}{dx} = -E(x) \tag{16}$$

where, ε_0 is the permittivity of free space and ε is the permittivity. We used formerly a two-dimensional field calculation code based on the Dynamic Alternating Direction Implicit (DADI) scheme. However, the computation time required for the field calculation was enormous and only a little time step for electron tracking was achieved. Then, we use the present 1D code to attain realistic time scale so that we can compare the results with experimental ones.

Figure 2 shows the flow chart of the present computation program. The interaction, which will occur for each particle is chosen randomly among the processes mentioned above. To reduce the computational cost, the cross sections are calculated in advance as a function of electron energy and the null-collision method is used in the Monte-Carlo scattering selection. Once the collision process is determined, the electron velocity vector and energy after collision are calculated based on the quantum theory. Using these position and velocity vectors, new position and velocity vectors after integration time τ are determined by eqs. (11)-(13). When an ion is generated due to

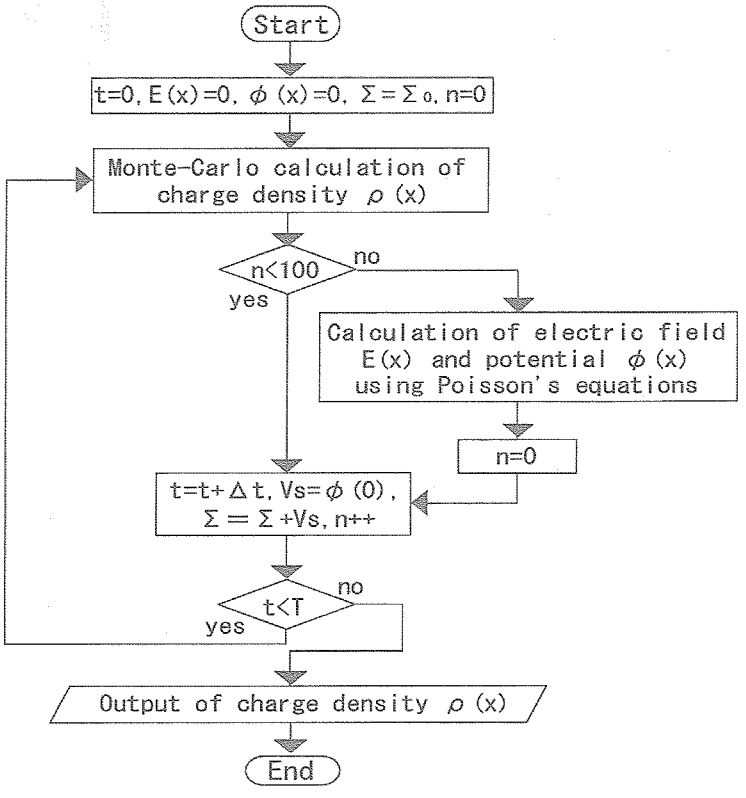

FIGURE 2. Flow chart of the program

the ionization collision, the positive ion charge is taken into account to the charge distribution. The one-dimensional charge distribution $\rho(x)$ is now obtained by projecting the three-dimensional charge distribution onto the one-dimensional mesh. The electric field calculation is currently executed in each 100 time integration steps because the induced field does not change during such a short time scale (100 times $\tau \approx 1 \times 10^{-15} = 1 \times 10^{-13}$ [sec]).

SIMULATION RESULTS

The simulated model is as shown in Fig. 1. The size of the film is 50 [μm] in x direction × 50 × 50 [μm] in y and z direction respectively. We used 50 mesh points in x (depth) direction resulting in grid spacing of 1 [μm]. The time step is set $\tau = 1.0 \times 10^{-15}$ [s] so that the most frequent collision can be taken into account. The density and relative permittivity of the Teflon film is 2.3×10^3 [kg/m^3] and 2.1 respectively. Electron beam is irradiated from above the film and the bottom surface is grounded. Incident electron energy and current density is 20 [keV] and 100 [A/cm^2] respectively. The boundary condition on the top surface is $E(0)=0$, and for the bottom surface $\phi(D)=0$.

Figure 3 shows the charge distributions inside the film at various times. The computation time is up until 1.0×10^{-12} [sec]. This is because the total number of electron and ion particle exceeded the maximum memory allowance of our current machine (single Pentium 4, 256 Mbyte). The time history of the number for each particle is shown in Fig. 4. The number of electron particle becomes 1.0×10^6 at the end of the computation. In addition, the number of Carbon ion grows rapidly far more than expected. This is because the Carbon ionization tends to occur frequently at the energy range tested. The total particle number becomes 2.0×10^6.

As seen in Fig. 3, the negative charge accumulation develops around the depth of 5 [μm]. And, the electrons are going to penetrate deeply into the film. The penetration depth at the end of the computation is about 30 [μm]. Frequent ionization near the irradiated surface creates a large number of Carbon and Fluorine ions resulting in the positive charge accumulation as seen in Fig. 3. The positive charge is higher than the negative charge induced by the accumulated electron. Figure 5 shows the time history of charge distribution owing to electron accumulation only. The accumulation peak resides at the depth of 3[μm] and the accumulation is developing as time goes. However, the maximum penetration depth seems to halt at 30 [μm]. The maximum penetration depth, called as range, is determined by the incident electron energy and 30 [μm] is the result for this test case. The penetration depth predicted by our simulation is about three times larger than Ref. [5]. The difference may be attributed to the estimation of the cross sections or velocity assignment after collision in our method.

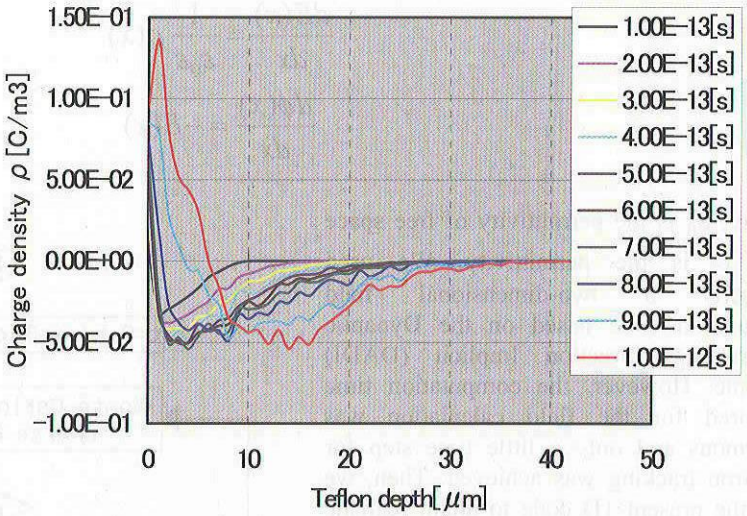

FIGURE 3. Charge distribution during irradiation

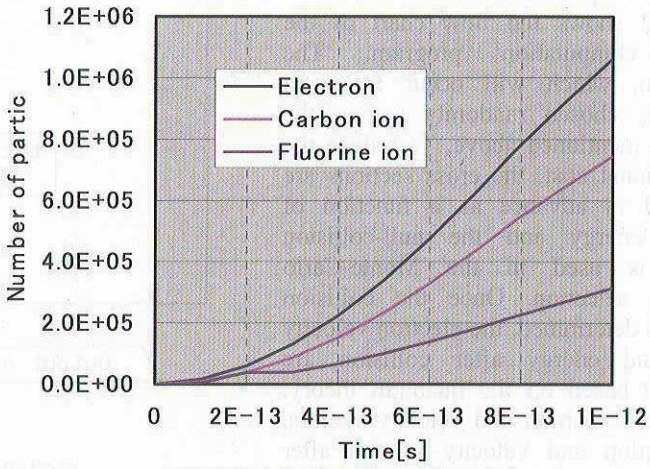

FIGURE 4. Numbers of particles

Figure 6 shows the time history of electric field distribution along the x direction calculated from the charge distribution in Fig. 3. Because of the negative charge accumulation due to the electron particles, the filed develops negatively until the time of 7.0×10^{-13} [sec]. Then, the field becomes

positive due to the accumulation of Carbon and Fluorine ions near the irradiated surface. The positive filed seems to be growing as time goes.

We attempted parallelization of the simulation code using the MPI methodology, but excessive data communication of particle attribution between processors made it difficult to efficient processor usage. Reorganization of data structure and its implementation to the program is underway.

ELECTRON IRRADIATION EXPERIMENTS ON DIELECTRIC FILMS

The experimental procedure and apparatus presented in [6] enables us to measure the charge distribution inside dielectric materials in real time during irradiation. The Piezo-electric Induced Pressure Wave Propagation (PIPWP) experimental procedure uses a pulsed pressure wave propagating in the sample as a charge probe [9]. When there are electric charges in the sample, the position of chares move slightly by the pressure wave. The movement of the charges induces the change of surface charges on the electrode that causes displacement current in the external circuit. The time-history of the displacement current indicates the charge distribution in the sample as described below for various materials.

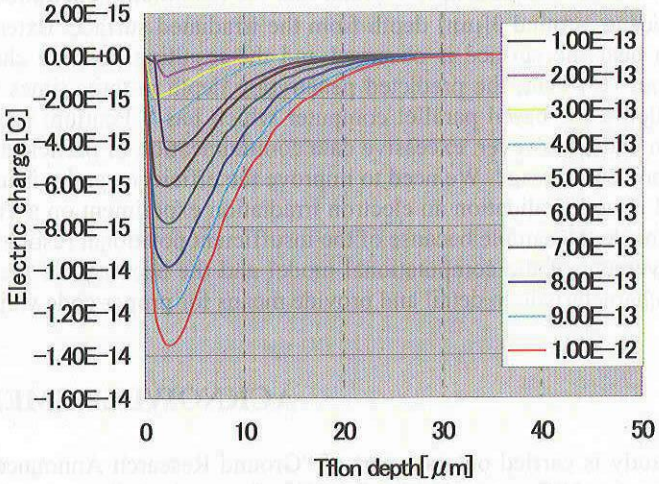

FIGURE 5. Charge distribution due to electron only

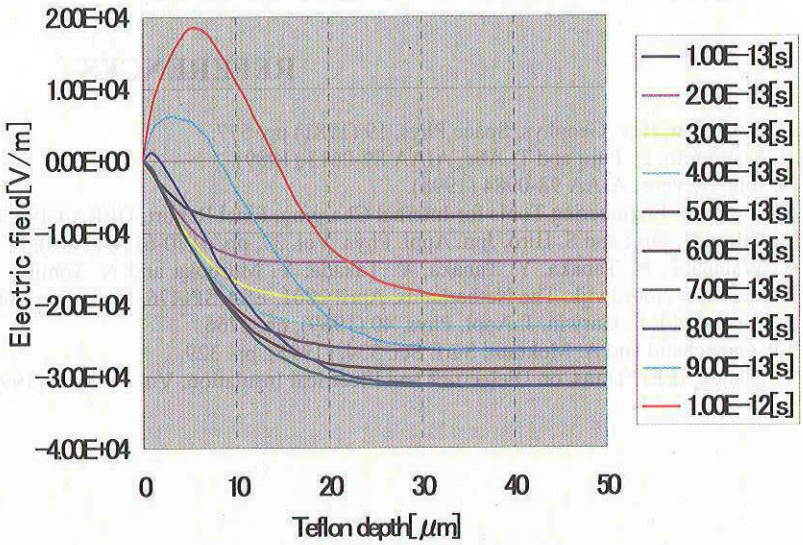

FIGURE 6. Electric field distribution during irradiation

Teflon Film

Figure 7 shows the charge density distribution inside a Teflon film with thickness of 190 μm. The incident electron energy is 90 keV and the current density is 205 nA/cm^2. The measurement was carried out after 10 minutes irradiation. Two charge peaks are found at the electrodes, but there is no apparent charge accumulation inside the film. The peak observed around 100 μm is not a significant signal. For the incident energy of 90 keV it was expected that the penetration depth was several dozen μm. But the positional resolution of our current device is 40 μm. Thus, electron deposition within a range of the positional resolution from the irradiated surface cannot be detected. The resolution can be improved by shortening the pulse width because it directly affects the detected signal. Experiments using shorter pulse are underway and the resolution will become high enough to detect shallow deposition.

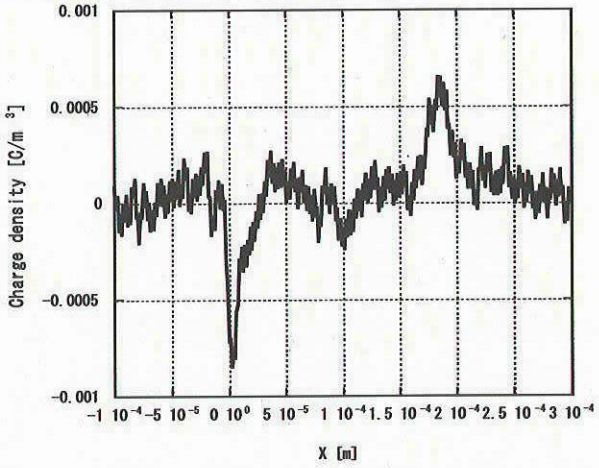

FIGURE 7. Experimental results of charge density in Teflon film

SUMMARY

The charge accumulation processes inside a Teflon film are investigated with one-dimensional Monte-Carlo simulation. Elastic and inelastic scattering processes are considered theoretically in the collisions between electrons and atoms consisting of Teflon® (CF4). Simulation results show the electron and ion deposition inside the film. Under the 20 [keV] electron irradiation, it is found that the maximum penetration depth is 30 [μm] and the accumulation peak of electron occurs around 3[μm] depth from the irradiated surface. Extensive Carbon and Fluorine ion generation due to ionization near the surface is observed and the resulting positive charge accumulation is clearly seen in the charge distribution. However, the predicted penetration depth is three times larger comparing with previous simulations [5]. We installed a PC-based parallel computer which has 8 Pentium processors and attempted the parallelization of the simulation code. However, excessive data communication of particle attribution between processors made it difficult to efficient processor usage. We need to improve the efficiency and it is underway.

To aid in code validation an electron irradiation experiment on a Teflon film is conducted but no clear deposition is detected inside the sample because of the insufficient positional resolution of our experimental system.

Improvement of the computational model and the accuracy of the experimental method are needed to discuss the charging characteristic in detail and provide means for proper code validation.

ACKNOWLEDGMENTS

This study is carried out as a part of "Ground Research Announcement for Space Utilization" promoted by Japan Space Forum and "Grant-in-Aid for Scientific Research (A)" promoted by Japan Society for the Promotion of Science.

REFERENCES

1. H. B. Garrett, Rev. Geophys. Space Phys, 19 (1981) pp. 577.
2. H. Nishimoto, H. Fujii and T. Abe, AIAA 89-0613 (1989).
3. N. John Stevens, AIAA 98-0984 (1998).
4. J. Sorensen, Engineering Tools for Internal Charging, Final Report, DERA/CIS/CIS2/CR990401, ESA No. 12115 (1999).
5. A. Palov, H. Fujii and S. Hiro, Jpn. Appl. Phys. Vol. 37, pp. 6170-6176 (1998).
6. R. Watanabe, H. Tanaka, Y. Tanaka, Y. Takada, Y. Murooka and N. Tomita, Proc. of 7th Spacecraft Charging Technology Conference, Noordwijk, The Netherlands, April 2001, ESA SP-476, November 2001, pp. 429.
7. J. Llacer and E.L. Garwin, J. Appl. Phys. 40 (1969), pp. 2766.
8. J.P. Ganachaud and A. Mokrani, Surf. Sci. 334, (1995), pp. 329.
9. T. Takada, IEEE Trans. on Dielectrics and Electrical Insulation, Vol. 6 No. 5, (1999), pp. 519.